PHYSICAL REVIEW D **85,** 026004 (2012)

Holographic zero sound at finite temperature

Richard A. Davison* and Andrei O. Starinets†

Rudolf Peierls Centre for Theoretical Physics, University of Oxford, 1 Keble Road, Oxford OX1 3NP, United Kingdom

(Received 5 October 2011; published 17 January 2012)

We use gauge-gravity duality to study the temperature dependence of the zero sound mode and the fundamental matter diffusion mode in the strongly coupled $\mathcal{N} = 4$ $SU(N_c)$ supersymmetric Yang-Mills theory with N_f $\mathcal{N} = 2$ hypermultiplets in the $N_c \gg 1$, $N_c \gg N_f$ limit, which is holographically realized via the D3/D7 brane system. In the high density limit $\mu \gg T$, three regimes can be identified in the behavior of these modes, analogous to the collisionless quantum, collisionless thermal, and hydrodynamic regimes of a Landau Fermi liquid. The transitions between the three regimes are characterized by the parameters T/μ and $(T/\mu)^2$, respectively, and in each of these regimes the modes have a distinctively different temperature and momentum dependence. The collisionless-hydrodynamic transition occurs when the zero sound poles of the density-density correlator in the complex frequency plane collide on the imaginary axis to produce a hydrodynamic diffusion pole. We observe that the properties characteristic of a Landau Fermi-liquid zero sound mode are present in the D3/D7 system despite the atypical T^6/μ^3 temperature scaling of the specific heat and an apparent lack of a directly identifiable Fermi surface.

DOI: 10.1103/PhysRevD.85.026004 PACS numbers: 11.25.Tq, 67.10.Jn, 71.10.Ay

I. INTRODUCTION

The AdS/CFT correspondence [1–4] and, more generally, gauge-gravity duality have been used extensively for studies of the thermodynamics and transport properties of strongly interacting quantum field theories at finite temperature and density. Applications of the correspondence to real-world physics initially concentrated on QCD and, in particular, the quark-gluon plasma [5,6], but in recent years there has been a surge of interest in using these tools to study the physics of condensed matter systems (see, e.g., [7–9] for an introduction to the field).

In this paper we investigate the behavior of the collective modes of the $\mathcal{N} = 4$ $SU(N_c)$ supersymmetric Yang-Mills theory coupled to N_f $\mathcal{N} = 2$ fundamental hypermultiplets at infinitely large 't Hooft coupling $\lambda = g_{\mathrm{YM}}^2 N_c$ in the limit $N_c \gg 1$, $N_c \gg N_f$, at finite temperature T and finite density of the fundamental matter d. The holographic dual of this theory is provided by embedding N_f D7-branes in the gravitational background created by N_c D3-branes and treating the D7-branes as probes [10]. Although a seemingly elaborate construction, this is one of the simplest known finite-density field theories for which an explicit dual is known, and it has some interesting properties.

At strictly zero temperature and zero hypermultiplet mass, the theory supports a collective excitation which appears as a pole in the density-density correlator [11]. Such an excitation, found in [11] using the dual gravity methods and thus referred to here as the "holographic zero sound," is reminiscent of the zero sound mode predicted to exist by Landau in a class of Fermi-liquid systems [12] (see also [13–17]) and subsequently observed in liquid helium-3 [18,19]. In Landau Fermi liquids (LFLs), the zero sound mode arises due to (nonthermal) interactions between the constituent fermions which result in oscillations of the Fermi surface. The holographic zero sound mode in the D3/D7 system at zero temperature has a speed equal to that of the ordinary (first) sound and an attentuation proportional to the square of the momentum. This is identical to what one finds in the Fermi-liquid models where the interaction strength (parametrized by the Fermi-liquid coefficient F_0) approaches infinity [16]. At the same time, the heat capacity of the D3/D7 system is proportional to T^6 at low temperatures whereas in normal Fermi liquids it is proportional to T.

Similar investigations have been made in other string-theoretic constructions—in [20] it was shown that the holographic zero sound mode persists at $T = 0$ when the hypermultiplet is given a finite mass, in [21] a similar mode was found in the $T = 0$ D4/D8/$\overline{\mathrm{D8}}$ theory at finite density, in [22] a "zero sound" mode was reported to exist in the $(1 + 1)$-dimensional theory on the D3/D3 intersection and in [23] a low temperature zero sound mode was found in the theory on the $(2 + 1)$-dimensional D3/D7 brane intersection. In the D4/D8/$\overline{\mathrm{D8}}$ case—where the only fundamental matter present is fermions—the heat capacity is proportional to T as expected for a Landau Fermi liquid. However, the imaginary part of the zero sound mode in this case has an unconventional q^3 dependence, which is at odds with the predictions of LFL theory. Holographic zero sound modes have also been discovered in theories consisting of probe Dirac-Born-Infeld (DBI) actions embedded in Lifshitz (i.e., nonrelativistic) spacetimes [24,25]. Such modes have a density-dependent speed, and their properties depend upon the critical exponent of the spacetime. In addition to these, the field theory dual to $(3 + 1)$-dimensional Einstein-Maxwell gravity with a

*r.davison1@physics.ox.ac.uk
†andrei.starinets@physics.ox.ac.uk

cosmological constant was found to support a long-lived sound mode at zero temperature [26].

A natural question to ask is what happens to the holographic zero sound mode when the temperature is turned on. In [27], it was argued that at any infinitesimal temperature the zero sound mode of the D3/D7 theory is no longer dominant and instead density transport occurs mainly via diffusion. In this paper we show that this is not the case—at low temperatures, the holographic zero sound mode still dominates the density-density correlator with a dispersion relation very similar to that at $T = 0$. Furthermore, we show (numerically) that the real part of this mode is independent of temperature whereas its imaginary part receives corrections proportional to T^2. At a sufficiently high temperature, there is a crossover to a hydrodynamic regime where the diffusion mode of [27] dominates (such crossovers are common, see [28–33] for other holographic examples of this). This behavior is familiar as it is the same as that predicted by Landau's theory of Fermi liquids, to which we now turn to help clarify these results and to identify the relevant scales involved.

In Landau's theory of Fermi liquids, one assumes that the ground state is a degenerate system of interacting fermionic quasiparticles. The theory describes small fluctuations around this ground state due to quasiparticle-quasihole excitations and/or collective excitations, and remains valid as long as these fluctuations are sufficiently small. The applicability conditions of Landau Fermi-liquid theory are given by the inequalities

$$T \ll \mu, \qquad \omega \ll \mu, \tag{1}$$

where $\mu \sim d^{1/3}$ is the chemical potential. The first inequality guarantees that we are considering a degenerate (i.e., quantum) liquid, while the second ensures that the excitations are sufficiently macroscopic, i.e., their wavelengths are much larger than the characteristic interparticle distance (this condition also implies that the quasiparticles remain sufficiently close to the Fermi surface $\omega \sim |\epsilon_p - \mu| \ll \mu$). The results of the Landau theory can be viewed as the leading order term in an expansion in powers of ω/μ [13,16].

In Fermi liquids, the zero sound mode is a longitudinal, gapless, collective excitation corresponding to oscillations of the Fermi surface around its equilibrium shape at zero temperature. Its dispersion relation $\omega(q) = v_s q - i\Gamma_\omega$ contains a nonzero damping due to the mode's decay into quasiparticle-quasihole pairs. It is often more convenient to work with real frequency and complex wave vector $q(\omega) = \omega/v_s + i\Gamma_q$. The damping rate is conveniently characterized by considering the argument of q, $\arg q(\omega) = \mathrm{Im}q/\mathrm{Re}q$, as a function of the frequency.

The zero sound mode persists at small, nonzero temperatures as well, but its properties are altered by the thermal collisions of the quasiparticles. Such collisions have a characteristic frequency $\nu \sim 1/\tau$, where τ is the mean time between quasiparticle collisions. One distinguishes three regimes: the hydrodynamic regime, characterized by $\omega \ll \nu$; the collisionless thermal (classical) regime, with $\omega \gg \nu$, $\omega \ll T$; and the collisionless quantum regime, $\omega \gg \nu$, $\omega \gg T$. The zero-temperature zero sound mode persists essentially unaltered in the collisionless quantum regime, where thermal excitations are too weak and infrequent to influence it. As the temperature is increased, however, thermal excitations change the attenuation of the zero sound mode giving it nontrivial temperature dependence. In the hydrodynamic regime, thermal excitations destroy the zero sound mode completely. However, these excitations support the ordinary hydrodynamic sound mode with viscous damping, and the thermal diffusion mode.

In the collisionless regime, the frequency ν can be computed from kinetic theory applied to Fermi liquids [13,14,16]:

$$\nu \sim \frac{\pi^2 T^2 + \omega^2}{\varepsilon_F (1 + e^{-\omega/T})}, \tag{2}$$

where $\varepsilon_F \sim \mu$. The decay rate of the zero sound mode in the collisionless regime is $\Gamma_q \sim \nu$ [16]. In the quantum collisionless regime one has then $\Gamma_q \sim \omega^2/\mu$ and $\arg q(\omega) \sim \omega/\mu$, whereas in the thermal collisionless regime $\Gamma_q \sim T^2/\mu$ and $\arg q(\omega) \sim (T/\mu)^2 \mu/\omega$. Finally, in the hydrodynamic regime, the conditions $\omega \ll \nu$ and $\omega \ll T$ lead to $\omega/\mu \ll (T/\mu)^2$ [the "quantum" limit $\omega \gg T$, $\omega \ll \nu$ lies outside of the LFL applicability range (1)]. The attenuation of hydrodynamic (first) sound is determined by the viscosity and is proportional to ω^2/T^2 [13,14,16].

The dimensionless variables which are most convenient for identifying the three regimes are ω/μ and q/μ. In these variables, regions I, II, and III corresponding to the hydrodynamic, collisionless thermal, and collisionless quantum regimes, respectively, are separated by the scales $(T/\mu)^2$ and T/μ. Alternatively, in the language of the "traditional" hydrodynamic variables ω/T and q/T, the relevant scales are T/μ, 1, and μ/T (see Table I and Fig. 1).

The sound attenuation constants in various regimes are shown in Table II and Fig. 2. The temperature dependence of the sound attenuation coefficient Γ_q is shown in Fig. 3. We shall use this information as a suggestive guide in our

TABLE I. Relative scales in a Landau Fermi liquid.

	ω/μ, q/μ variables	ω/T, q/T variables
Hydrodynamic regime	$\frac{\omega}{\mu} \ll (\frac{T}{\mu})^2$	$\frac{\omega}{T} \ll \frac{T}{\mu}$
Collisionless thermal regime	$(\frac{T}{\mu})^2 \ll \frac{\omega}{\mu} \ll \frac{T}{\mu}$	$\frac{T}{\mu} \ll \frac{\omega}{T} \ll 1$
Collisionless quantum regime	$\frac{T}{\mu} \ll \frac{\omega}{\mu} \ll 1$	$1 \ll \frac{\omega}{T} \ll \frac{\mu}{T}$

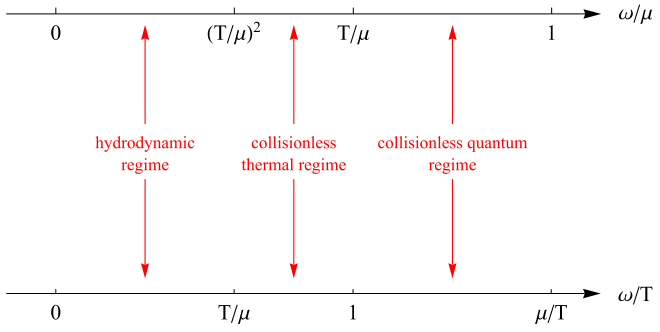

FIG. 1 (color online). Relative scales in the hydrodynamic, collisionless thermal and collisionless quantum regimes of a Landau Fermi liquid.

investigation of the holographic zero sound at finite temperature.

In the massless D3/D7 system at low temperature, the chemical potential is proportional to the cubic root of the volume density d of the $U(1)$ "baryon" charge[1] [11]

$$\mu = \alpha d^{1/3}\left(1 + O\left(\frac{T}{d^{1/3}}\right)\right), \tag{3}$$

where α can be expressed using the Euler beta function, $\alpha = B(1/3, 7/6)/2 \approx 1.402$. We shall study the D3/D7 theory in the limit $T \ll d^{1/3}$, $\omega \ll d^{1/3}$ formally corresponding to the applicability regime (1) of Landau Fermi-liquid theory. The appropriate dimensionless variables are

$$\bar{\omega} = \frac{\omega}{d^{1/3}}, \qquad \bar{q} = \frac{q}{d^{1/3}}, \qquad \tilde{d} = \frac{d}{(\pi T)^3}. \tag{4}$$

A priori, we do not expect to find agreement with the LFL results outlined above since the D3/D7 system appears to be microscopically rather different, with no obviously detectable Fermi surface or long-lived quasiparticles in its vicinity. Nevertheless, we do find that the behavior of the zero sound mode at finite temperature is qualitatively similar to the one predicted (and observed) in a Landau Fermi liquid:

(i) The three regimes (hydrodynamic, collisionless thermal, and collisionless quantum) are readily identified by analyzing the behavior of the lowest quasinormal frequencies and the spectral function of the charge density correlator. The collisionless-hydrodynamic thermal transition occurs at $\bar{\omega}\tilde{d}^{2/3} \sim 1$ and is most spectacularly manifested in the motion of the zero sound poles in the complex frequency plane: as the temperature is increased, the two poles (corresponding to zero sound propagation with velocities $+v_s$ and $-v_s$ in the field theory) recede into the complex plane, approximately tracing a circle, until they collide on the imaginary axis and form two poles with zero real part; one of these new poles recedes even deeper into the complex plane while the other approaches the origin. The latter pole is the charge density diffusion mode (with the diffusion constant computed in [27,35]) characteristic of the hydrodynamic regime. Such behavior was previously observed in [31] and also in a $(2+1)$-dimensional holographic field theory in [23], where it was correctly identified as the collisionless-hydrodynamic transition involving the zero sound mode. A similar transition between propagating and diffusive modes has been seen in a model of a holographic superconductor [33]. The second transition, between the collisionless thermal and the collisionless quantum regimes, is observed at $\bar{\omega}\tilde{d}^{1/3} \sim 1$.

As our investigation is limited to the current-current correlators, we are not able to follow the emergence of first sound in the hydrodynamic regime; this should appear as a pole in the energy-momentum tensor correlators of the field theory which are decoupled from the current-current correlators in the probe brane limit. Accordingly, we do not expect the details of the collisionless-hydrodynamic thermal transition described above to survive beyond the probe brane approximation: it seems more likely that the acoustic poles, rather than colliding on the

TABLE II. Sound attenuation coefficients in a Landau Fermi liquid.

	Γ_ω	Γ_q	$\arg q$
Hydrodynamic regime	$(\frac{\mu}{T})^2 \frac{q^2}{\mu}$	$\frac{\mu\omega^2}{T^2}$	$(\frac{\mu}{T})^2 \frac{\omega}{\mu}$
Collisionless thermal regime	$\frac{T^2}{\mu}$	$\frac{T^2}{\mu}$	$(\frac{T}{\mu})^2 \frac{\mu}{\omega}$
Collisionless quantum regime	$\frac{q^2}{\mu}$	$\frac{\omega^2}{\mu}$	$\frac{\omega}{\mu}$

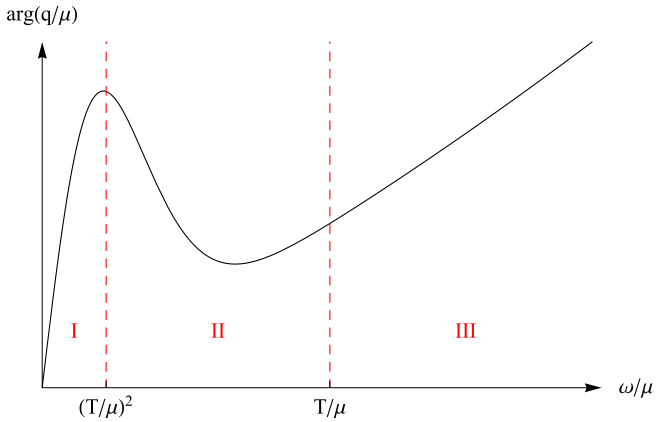

FIG. 2 (color online). A sketch of the dependence of the sound mode damping on frequency in the hydrodynamic (I), collisionless thermal (II), and collisionless quantum (III) regimes of a Landau Fermi liquid. First sound propagates in region I while the zero sound mode exists in regions II and III.

[1]An explicit expression for the charge density operator involving fundamental fermions and complex scalars of the $\mathcal{N} = 2$ hypermultiplet is given in Appendix A of [34].

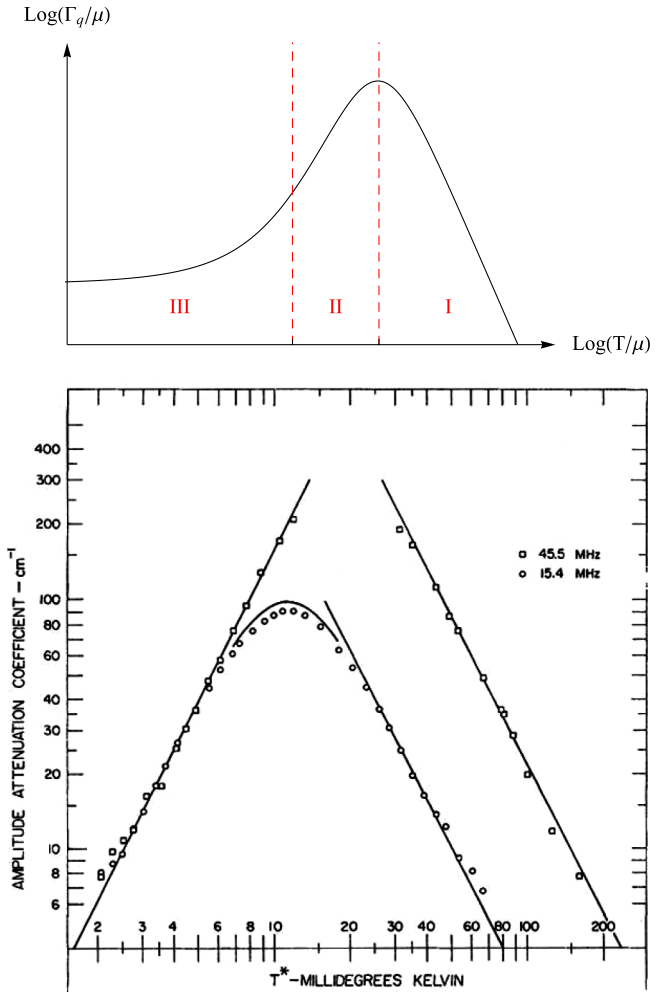

FIG. 3 (color online). The temperature dependence of the sound attenuation coefficient Γ_q in various regimes of a Landau Fermi liquid. Top panel: A sketch of the dependence in the hydrodynamic (I), collisionless thermal (II), and collisionless quantum (III) regimes. Bottom panel: Temperature dependence of the acoustic attenuation in liquid ^{3}He at $P = 32$ kPa measured at both 15.4 MHz (○) and 45.5 MHz (□). The lines through the data correspond to $\log\Gamma_q \sim 2\log T$ and $\log\Gamma_q \sim -2\log T$ in the collisionless thermal and hydrodynamic regimes, respectively, in agreement with Table II.

imaginary axis as the temperature is raised, will recede deeper into the complex plane, reflecting the behavior of the attenuation curve in Fig. 3, and then come back close to the real axis again as the hydrodynamic sound poles.

(ii) The D3/D7 zero sound attenuation coefficients exhibit the momentum, temperature, and density dependence typical of a Landau Fermi liquid as shown in Table II. We find that the dependence of the acoustic damping upon frequency and temperature is qualitatively the same as shown in Figs. 2 and 3 in regions II and III.

(iii) These results remain valid in the case of a nonvanishing hypermultiplet mass (within the region of thermodynamic stability of the theory).

The structure of the paper is as follows. In Sec. II, we give a brief description of the gravitational dual of the D3/D7 field theory and the relevant, known properties of its Green's functions and spectral functions. In Sec. III we present our numerical results for the density-density spectral function (and the dominant pole of the corresponding Green's function) when $T \ll d^{1/3}$. We identify the three regimes similar to those of a Landau Fermi liquid, and describe in detail the behavior of the collective modes as the temperature of the system is varied. We summarize our results and discuss how they may generalize to other holographic finite-density systems in Sec. IV. Some details relevant for the case of a massive hypermultiplet are relegated to appendixes: Appendix A contains the action and equations of motion for the fluctuations, and Appendix B provides a derivation of the zero sound attenuation constant at zero temperature.

II. THE D3/D7 SYSTEM

The specific field theory whose elementary excitations at finite temperature and density we wish to investigate is $(3+1)$-dimensional $\mathcal{N} = 4$ $SU(N_c)$ supersymmetric Yang-Mills theory coupled to N_f $\mathcal{N} = 2$ fundamental hypermultiplets with a global $U(N_f)$ flavor symmetry. It arises as the low-energy theory on the world volume of a set of N_c D3-branes and N_f D7-branes intersecting along $(3+1)$ dimensions. Taking $N_c \to \infty$ with both $\lambda = g_{\mathrm{YM}}^2 N_c$ and N_f/N_c fixed, and subsequently taking $\lambda \to \infty$ and $N_f/N_c \to 0$, we obtain a classical gravitational dual to this field theory [10,36]:

$$S = S_{\text{adjoint}} + S_{\text{fundamental}}, \\ = S_{\text{adjoint}} - N_f T_{\text{D7}} \int d^8\xi \sqrt{-\det(g_{ab} + F_{ab})}, \quad (5)$$

where S_{adjoint} is the ten-dimensional supergravity action and T_{D7} is the tension of a D7-brane. In this probe brane limit, the metric is fixed and it is $S_{\text{fundamental}}$ which contains the dynamical information. For a zero-temperature field theory, the contribution of the fundamental matter is the DBI action of N_f probe D7-branes extended along an $\mathrm{AdS}_5 \times S^3$ section of the (fixed) $\mathrm{AdS}_5 \times S^5$ background spacetime generated by the D3-branes. In Eq. (5), g_{ab} denotes the induced world volume metric on the D7-brane and F_{ab} is the field strength of a world volume $U(1) \subset U(N_f)$ gauge field.

When the field theory is at a nonzero temperature, the background spacetime is that of an AdS-Schwarzschild black brane (with a horizon at $r = r_H$) times a five-sphere:

$$ds_{10}^2 = \frac{r^2}{R^2}\left[-\left(1-\frac{r_H^4}{r^4}\right)dt^2 + d\vec{x}^2\right] + \left(1-\frac{r_H^4}{r^4}\right)^{-1}\frac{R^2}{r^2}dr^2 + R^2 ds_{S^5}^2. \quad (6)$$

The D7-brane wraps an asymptotically $AdS_5 \times S^3$ section of the metric, with the horizon radius of the background related to the temperature of the field theory via $T = r_H/\pi R^2$.

In terms of the dimensionless radial coordinate $u = r_H^2/r^2$, the metric (6) can be written as

$$ds_{10}^2 = \frac{(\pi T R)^2}{u}(-f dt^2 + d\vec{x}^2) + \frac{R^2}{4u^2 f}du^2 + R^2(d\theta^2 + \sin^2\theta ds_{S^1}^2 + \cos^2\theta ds_{S^3}^2), \quad (7)$$

where $f(u) = 1 - u^2$. In these coordinates, the horizon is located at $u = 1$ and the boundary at $u = 0$. In equilibrium, the D7-brane embedding can be characterized by a single embedding coordinate $\theta(u)$ (which determines which S^3 section of the background S^5 it wraps). The gauge field on the brane is dual to a global flavor current in the field theory and thus turning on the time component of a $U(1) \subset U(N_f)$ gauge field $A_t(u)$ on the brane corresponds to introducing a finite density d of the $U(1)$ ''baryon'' charge in the field theory. In this case, it corresponds to a net density of fundamental fermions and scalars.

The equations of motion for the background fields are obtained from the DBI action

$$S_{\text{fundamental}} = -\frac{N r_H^4}{2}\int_0^1 du d^4x \frac{\cos^3\theta}{u^3} \times \sqrt{1 + 4u^2 f\theta'^2 - 4\frac{u^3}{r_H^2}A_t'^2}, \quad (8)$$

where $N = N_f T_{D7} V_{S^3}$ is a normalization constant determined by the gauge-gravity duality dictionary [34] and primes denote derivatives with respect to u. One of the equations of motion derived from the action (8) reduces to

$$A_t'(u) = -\frac{r_H \tilde{d}}{2}\sqrt{\frac{1 + 4u^2 f(u)\theta'(u)^2}{\cos^6\theta(u) + \tilde{d}^2 u^3}}, \quad (9)$$

where $\tilde{d} \equiv dR^6/r_H^3 = d/(\pi T)^3$ is a dimensionless parameter of the field theory related to the net number density of ''quarks'' n_q in the field theory [2] via

$$\tilde{d} = \frac{2^{5/2} n_q}{\sqrt{\lambda} N_f N_c T^3}. \quad (10)$$

For a given density $\tilde{d}$, there is a corresponding dimensionless chemical potential given by

$$\tilde{\mu} = \frac{\tilde{d}}{2}\int_0^1 du \sqrt{\frac{1 + 4f(u)u^2\theta'(u)^2}{\cos^6\theta(u) + \tilde{d}^2 u^3}}, \quad (11)$$

which is related to the field theory chemical potential μ_{FT} by $\tilde{\mu} \equiv \mu/\pi T = \sqrt{(2/\lambda)}(\mu_{\text{FT}}/T)$. In the massless case, the integral in Eq. (11) can be computed exactly [11]: it reduces to (3) in the low temperature limit. The important scaling [not entirely obvious from Eq. (11) and generically accompanied by mass and temperature corrections [11,37]] to emphasize is

$$\frac{\mu}{T} \sim \tilde{\mu} \sim \tilde{d}^{1/3}. \quad (12)$$

The equation of motion for the embedding coordinate is

$$\frac{d}{du}\left(\frac{f(u)\cos^3\theta(u)\theta'(u)}{u\sqrt{G(u)}}\right) + \frac{3\cos^2\theta(u)\sin\theta(u)\sqrt{G(u)}}{4u^3} = 0, \quad (13)$$

where

$$G(u) = \cos^6\theta(u)\frac{1 + 4u^2 f(u)\theta'(u)^2}{\cos^6\theta(u) + u^3\tilde{d}^2}.$$

Equation (13) has no known generic analytic solution and must be solved numerically.[3] Near the boundary, the solution has the form

$$\theta(u) = \frac{\tilde{m}}{\sqrt{2}}\sqrt{u} + \cdots, \quad (14)$$

where $\tilde{m}$ is related to the bare mass[4] of the fundamental matter in units of temperature via [39]

$$\tilde{m} = \frac{2}{\sqrt{\lambda}}\frac{M_q}{T}. \quad (15)$$

To study the temperature dependence of the theory at finite density, it will be more convenient to use the field theory mass normalized with respect to density rather than temperature:

$$\bar{m} = \frac{\tilde{m}}{\tilde{d}^{1/3}} = \frac{2\pi}{\sqrt{\lambda}}\frac{M_q}{d^{1/3}}. \quad (16)$$

Note that $\theta(u) = 0$ for a massless hypermultiplet, and thus the dual description greatly simplifies in this case; there is only one nontrivial background field $A_t(u)$ which has the simple equation of motion

[2] See footnote 1. Note that our normalization of d is different from the one used in [34]: in [34], $d \sim n_q$, whereas in our case $d \sim n_q/\sqrt{\lambda} N_c N_f$.

[3] A method to approximate the solution in the low temperature limit has been proposed in [38].

[4] The explicit field theory ''quark'' mass operator is given in Appendix A of [34].

$$A_t'(u) = -\frac{r_H \tilde{d}}{2}(1+\tilde{d}^2u^3)^{-1/2}. \tag{17}$$

The thermodynamics of the system can be determined by computing the on-shell action. In the massless case, the specific heat schematically has the following temperature dependence [11]:

$$c_V \sim N_c^2 T^3 + \cdots + \lambda N_f N_c T^6/d + \cdots, \tag{18}$$

where the first term comes from the adjoint $\mathcal{N}=4$ supersymmetric Yang-Mills degrees of freedom. The pressure P, the entropy density s, and the energy density ε can be computed from the thermodynamic potential $\Omega(\mu, T)$ given explicitly in [11]: the entropy density is finite in the $T \to 0$ limit, $s \sim \mu^3$, and the equation of state is $\varepsilon = 3P$ for all T and μ (and thus the speed of first sound is $v_s = 1/\sqrt{3}$). In certain regimes, the system becomes thermodynamically unstable: there appears to be an instability at low density $\tilde{d} < \tilde{d}_c \approx 0.003\,15$ [32,34], and at high density and large mass $\bar{m} \gg 1$, $\tilde{d} \gg 1$ [38]. In addition, when $d \neq 0$ and $m \neq 0$ there is a lower limit on the possible value of μ, below which there is a phase transition to a Minkowski embedding with $d=0$ [37,40–43]. The values of the parameters considered in this paper are outside of these regimes.

To determine the field theory excitations, one considers fluctuations of the background bulk fields

$$\begin{aligned} \theta(u) &\to \theta(u) + \phi(u, z, t), \\ A_t(u) &\to A_t(u) + a_t(u, z, t), \\ A_i(u) &\to a_i(u, z, t), \end{aligned} \tag{19}$$

$i = x, y, z$, where we have chosen the fluctuations to depend on time, the radial coordinate and one of the spatial coordinates (z) only (the latter is possible due to the isotropy of the theory). Introducing Fourier components for the embedding fluctuation

$$\phi(u, z, t) = \int \frac{d\omega dq}{(2\pi)^2} e^{-i\omega t + iqz} \tilde{\phi}(u, \omega, q), \tag{20}$$

and similarly for $a_\mu(u, z, t)$, and expanding the DBI action (8) to quadratic order in fluctuations, one finds the resulting action and the corresponding equations of motion. The transverse modes $\tilde{a}_x$, $\tilde{a}_y$ decouple from the longitudinal modes $\tilde{a}_t$, $\tilde{a}_z$, and $\tilde{\phi}$. In the following, we shall focus on the longitudinal modes as they are the ones that encode the fate of zero sound at finite temperature.

For a nonzero hypermultiplet mass, the equations of motion lead to a pair of coupled differential equations for the embedding fluctuation $\tilde{\phi}(u, \bar{\omega}, \bar{q})$ and the gauge-invariant combination (cf. [44])

$$\bar{Z}(u, \bar{\omega}, \bar{q}) = \bar{\omega}\tilde{a}_z(u, \bar{\omega}, \bar{q}) + \bar{q}\tilde{a}_t(u, \bar{\omega}, \bar{q}), \tag{21}$$

where the dimensionless variables $\bar{\omega}$ and $\bar{q}$ were introduced in Eq. (4). The equations of motion and the action for the longitudinal fluctuations are given in Appendix A.

In the zero mass limit, the equations for these two modes decouple and the gauge-invariant combination (21) obeys the equation of motion

$$\frac{d}{du}\left[\frac{f(u)\bar{Z}'}{\sqrt{g(u)}(\bar{\omega}^2 - \bar{q}^2 f g)}\right] + \frac{\tilde{d}^{(2/3)}\bar{Z}}{4u\sqrt{g(u)}f(u)} = 0, \tag{22}$$

where $g(u) = (1+\tilde{d}^2u^3)^{-1}$. In this limit, the longitudinal part of the on-shell action is

$$S^{(2)}_{\text{long}} = N r_H^2 \int \frac{d\omega dq}{(2\pi)^2} \frac{f\bar{Z}(u, -\bar{\omega}, -\bar{q})\bar{Z}'(u, \bar{\omega}, \bar{q})}{\sqrt{g}(\bar{\omega}^2 - \bar{q}^2 f g)} \Big|_{u_H}^{u_B}. \tag{23}$$

In this massless case, we obtain the longitudinal retarded Green's functions from the gravitational fields via the usual procedure [45]

$$G^R_{J^z J^z}(\bar{\omega}, \bar{q}) = -\lim_{\epsilon \to 0} 2N r_H^2 \frac{\bar{\omega}^2}{\bar{\omega}^2 - \bar{q}^2} \frac{\bar{Z}'(\epsilon, \bar{\omega}, \bar{q})}{\bar{Z}(\epsilon, \bar{\omega}, \bar{q})}, \tag{24}$$

where the $-\bar{\omega}^2$ factor comes from the definition (21), and $\bar{Z}(u, \bar{\omega}, \bar{q})$ is the solution obeying ingoing boundary conditions at the horizon: $\bar{Z}(u, \bar{\omega}, \bar{q}) \sim (1-u)^\gamma$ as $u \to 1$, where $\gamma = -i\bar{\omega}\tilde{d}^{1/3}/4$. Poles of the retarded Green's function are determined by the values of $\bar{\omega}(\bar{q})$ for which the solution obeying the ingoing condition at the horizon vanishes at the boundary [44,45]. The density-density correlation function follows trivially from the conservation of current $G^R_{J^t J^t}(\bar{\omega}, \bar{q}) = \bar{q}^2 G^R_{J^z J^z}/\bar{\omega}^2$ and has the same poles as the longitudinal Green's function (24). The spectral functions of these operators are then obtained by taking the imaginary part:

$$\begin{aligned} \chi_{zz}(\bar{\omega}, \bar{q}) &= -2\,\text{Im}[G^R_{J^z J^z}(\bar{\omega}, \bar{q})], \\ \chi_{tt}(\bar{\omega}, \bar{q}) &= -2\,\text{Im}[G^R_{J^t J^t}(\bar{\omega}, \bar{q})], \end{aligned} \tag{25}$$

with $\chi_{tt} = \bar{q}^2\chi_{zz}/\bar{\omega}^2$. At zero temperature and density, the form of the longitudinal spectral function is known analytically [46]:

$$\chi_{zz}(\omega, q) = \frac{N_f N_c}{4\pi}(\omega^2 - q^2)\Theta(\omega^2 - q^2)\text{sgn}\omega, \tag{26}$$

where Θ is the Heaviside step function.

In the $\bar{m} \neq 0$ case, the coupled equations of motion for bulk fluctuations imply that the dual field theory operators mix and the method to determine the retarded Green's functions is more involved (see Appendix A for details).

At zero mass, high densities $\omega, q \ll d^{1/3}$ and strictly zero temperature, the dominant pole of the correlators $G^R_{J^t J^t}$ and $G^R_{J^z J^z}$ has the dispersion relation [11,47]

$$\bar{\omega} = \pm \frac{\bar{q}}{\sqrt{3}} - i \frac{\Gamma(\frac{1}{2})}{\Gamma(\frac{1}{6})\Gamma(\frac{1}{3})} \bar{q}^2 + O(\bar{q}^3). \tag{27}$$

This corresponds to a collective excitation of the system—the holographic zero sound mode. Its speed is equal to that of hydrodynamic sound, and it has an imaginary part $\propto q^2$. In the hydrodynamic limit $\omega, q \ll T$ the dominant pole is a purely imaginary pole with the Fickian diffusion dispersion relation

$$\bar{\omega} = -iD\bar{q}^2 + O(\bar{q}^3), \tag{28}$$

where the diffusion constant is given by [27,35]

$$D(\tilde{d}) = \frac{\tilde{d}^{1/3}}{2} \sqrt{1 + \tilde{d}^2}\, {}_2F_1\left[\frac{3}{2}, \frac{1}{3}; \frac{4}{3}; -\tilde{d}^2\right]. \tag{29}$$

Between these two extreme temperature limits, the poles of the Green's functions are not known analytically.

These results were generalized to the case of a massive hypermultiplet in [20,35]. The zero sound mode (27) persists when the hypermultiplet has a finite mass m, although the dispersion relation is altered to

$$\bar{\omega} = \pm \frac{1}{\sqrt{3}} \left(\frac{1 - \mathfrak{m}^2}{1 - \mathfrak{m}^2/3}\right)^{1/2} \bar{q} - i \frac{\Gamma(\frac{1}{2})}{\Gamma(\frac{1}{3})\Gamma(\frac{1}{6})} \frac{(1 - \mathfrak{m}^2)^{4/3}}{(1 - \mathfrak{m}^2/3)^2} \bar{q}^2 + O(\bar{q}^3), \tag{30}$$

where $\mathfrak{m} = \tilde{m}/\sqrt{2}\tilde{\mu} = M_q/\mu$. The real part of the dispersion relation (30) was obtained in [20] and the attenuation is derived in Appendix B. In the hydrodynamic limit, there is again a diffusion pole (28) whose diffusion constant can be derived via an Einstein relation [35]

$$D(\tilde{d}) = \frac{\tilde{d}^{1/3}}{2} \sqrt{\tilde{d}^2 + \cos^6\theta(1)} \int_0^1 du \frac{G(u)^{3/2}}{\cos^3\theta(u) H(u)} \times \left[1 + \tilde{d}\left(\frac{4f(u)u^2\theta'(u)}{G(u)\cos\theta(u)} \frac{\partial}{\partial \tilde{d}} [\cos\theta(u)\theta'(u)] + \frac{\sin\theta(u)}{\cos^2\theta(u)} \left(3 + \frac{4f(u)u^2\theta'(u)^2}{G(u)}\right) \frac{\partial}{\partial \tilde{d}} \sin\theta(u)\right)\right], \tag{31}$$

where $G(u)$ and $H(u)$ are defined in Appendix A.

At finite hypermultiplet mass, the D3/D7 system has nontrivial bound states analogous to mesons [36]. These bound states are visible as peaks of the spectral function. When $d = 0$, such modes exist only for large enough values of $\tilde{m} \propto M_q/T$ [39,46,48–50]. When $d \neq 0$, it seems that necessary conditions for their existence are large values of $\tilde{m}$ and small enough values of q/T and $d^{1/3}/T$ [31,32,51–53]. This is outside of the regime of our current interest. A full numerical analysis of the quasinormal modes of the theory when $T = 0$ is given in [54].

III. THE HIGH DENSITY REGIMES OF D3/D7 FUNDAMENTAL MATTER

In this section, we explore the behavior of the collective modes of the D3/D7 system in the low temperature regime $\tilde{d} \gg 1$ ($T \ll \mu$). Anticipating behavior similar to that observed in a Landau Fermi liquid, we expect the system to exhibit the three regimes shown in Fig. 1, and indeed we do find them. We investigate this by computing numerically the spectral functions and the poles of the Green's functions using the approach of [31,45]. This approach provides a numerical consistency check (invariance under radial translations) which we used to ensure our results were accurate. We always plot the normalized spectral functions such as $\chi_{zz}(\bar{\omega}, \bar{q})/2N_f N_c T^2 \bar{\omega}^2$: dividing by $\bar{\omega}^2$ has the advantage of reducing the high frequency asymptotics (26) to a constant.

A. The collisionless quantum regime

The collisionless quantum regime corresponds to $\bar{\omega}$ and $\bar{q}$ being in the interval

$$\tilde{d}^{-1/3} \ll \bar{\omega}, \bar{q} \ll 1, \tag{32}$$

see Eq. (12), Fig. 1, and Table I. We start by fixing a large value of $\tilde{d}$, for example, $\tilde{d} = 10^6$, and computing the longitudinal spectral function at a fixed momentum $\bar{q}$ in the interval (32), e.g., $\bar{q} = 0.4$. An isolated peak corresponding to the holographic zero sound mode in this low temperature regime is clearly visible in Fig. 4. Thus the zero sound mode persists at low but nonzero temperatures, contrary to the assertion in [27] that an infinitesimal temperature in the field theory will lead to diffusive transport.

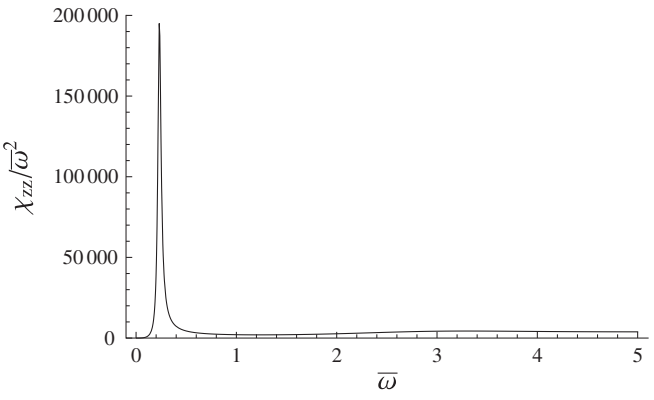

FIG. 4. The holographic zero sound peak in the collisionless quantum regime. The longitudinal spectral function is shown at $\tilde{m} = 0$, $\tilde{d} = 10^6$, and $\bar{q} = 0.4$.

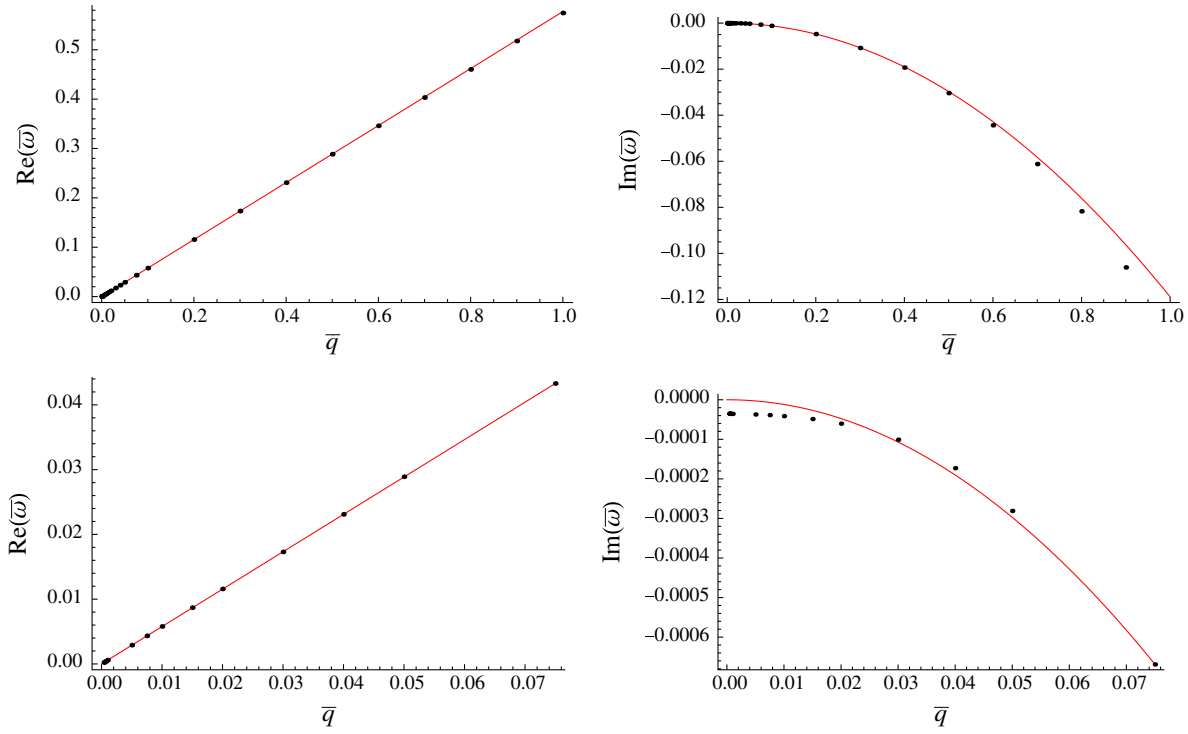

FIG. 5 (color online). The dispersion relation of the dominant pole at $\bar{m} = 0$, $\tilde{d} = 10^6$. Dots show numerical results at low T and the solid lines are the analytic result (27) at $T = 0$. The lower two graphs zoom in to the low $\bar{q}$ regions of the upper two.

By varying $\bar{q}$ (while keeping $\tilde{d}^{1/3}$ fixed), we can determine the dispersion relation of this collective mode at low temperature. Figure 5 shows the real and imaginary parts of the zero sound dispersion relation $\bar{\omega} = \bar{\omega}(\bar{q})$ at $\bar{m} = 0$, $\tilde{d} = 10^6$. Our numerical results are shown as dots and the solid lines correspond to the zero-temperature dispersion relation (27). We observe that in the collisionless quantum regime (32) the real part of the zero sound dispersion relation shows no noticeable deviation from the zero-temperature result (27). The imaginary part shows a close agreement with the zero-temperature result over the parameter range (32). Visible deviations from the zero-temperature result are apparent at very small ($\bar{q} \lesssim 0.02 \sim \tilde{d}^{-1/3}$) and very large ($\bar{q} \gtrsim 0.7$) momenta close to the boundaries of the interval (32). Note that although the imaginary part appears to be tending to a constant at small $\bar{q}$, this is only true up until the crossover to the hydrodynamic regime occurs, after which we obtain a diffusive mode. This crossover will be discussed in detail later in this section. At large momentum, the system is entering the low temperature, low density regime $\tilde{d}^{-1/3} \ll 1 \ll \bar{\omega}, \bar{q}$ (i.e., $\omega, q \gg d^{1/3} \gg T$), where the zero sound mode becomes very short lived as the corresponding pole recedes deep into the complex plane. As shown in Fig. 6, the zero sound peak in the spectral function gradually disappears in this regime, and the spectral function approaches the $d = 0$, $T = 0$ result (26).

At finite hypermultiplet mass, the results are qualitatively similar.[5] The longitudinal spectral functions show a lone peak[6] (similar to the one shown in Fig. 4) for values of $\bar{\omega}$ in the range (32). As shown in Fig. 7, the real part of the dispersion relation is essentially identical to the zero-temperature result (30), and the imaginary part deviates from the zero-temperature dependence given in (30) only at the boundaries of the interval (32).

It is interesting to note that the zero sound mode exists for all (numerically accessible) values of $\bar{m}$, including those for which $\tilde{m} \propto M_q/T \ll 1$. Thus the high density and low temperature interval in which the $T = 0$ zero sound mode persists is the same as in the massless case [given by the inequality (32)], i.e., we do not have to take the limit $M_q/T \to \infty$ which would be the genuine zero-temperature limit of the entire system.

[5]Technically, the massive case is more complicated as it involves solving a pair of coupled differential equations, with coefficients that depend upon the numerically computed embedding function. Because of numerical instability, we were not able to obtain accurate results for $\tilde{d} > 10^5$ and masses outside the interval $0.002 \lesssim \bar{m} \lesssim 1.68$ (at $\tilde{d} = 10^5$). We believe this limitation demonstrates the lack of our numerical skills rather than an effect of any physical significance.

[6]Peaks corresponding to "meson" bound states may exist for higher values of $\bar{\omega}$. We have not investigated this issue.

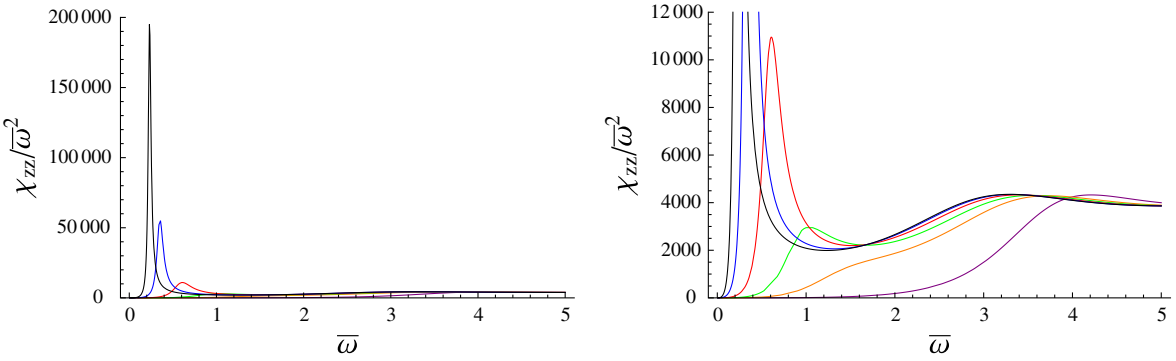

FIG. 6 (color online). The longitudinal spectral function at $\bar{m} = 0$, $\tilde{d} = 10^6$. Moving from left to right corresponds to increasing momentum: $\bar{q} = 0.4$ (black), 0.6 (blue), 1.0 (red), 1.5 (green), 2.0 (orange), 3.0 (purple).

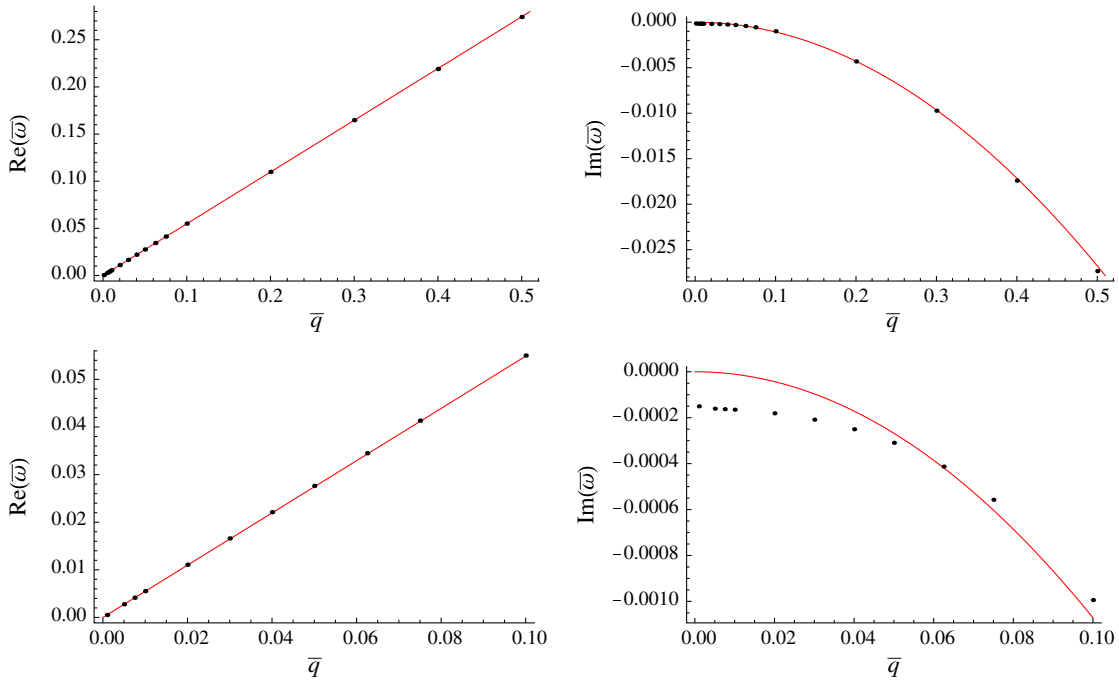

FIG. 7 (color online). The holographic zero sound dispersion relation for $\bar{m} = 0.76$, $\tilde{d} = 10^5$. Dots show numerical results at low T and the solid lines show the analytic result (27) at $T = 0$. The lower two graphs zoom in to the low $\bar{q}$ regions of the upper two.

B. The collisionless thermal regime

Having established the existence of a holographic zero sound mode at finite temperature, we now investigate the dependence of its velocity and attenuation on temperature, density, momentum, and mass. The collisionless thermal regime corresponds to excitations with $\bar{\omega}$ and $\bar{q}$ in the interval

$$\tilde{d}^{-2/3} \ll \bar{\omega}, \bar{q} \ll \tilde{d}^{-1/3}. \tag{33}$$

As discussed in Sec. III A, the imaginary part of the dispersion relation $\bar{\omega} = \bar{\omega}(\bar{q})$ for the zero sound shows significant deviations from the zero temperature $\sim \bar{q}^2$ behavior in the region $\bar{q} \lesssim \tilde{d}^{-1/3}$. Investigating this further, one can see that in the interval $\tilde{d}^{-2/3} \lesssim \bar{q} \lesssim \tilde{d}^{-1/3}$ the imaginary part $\mathrm{Im}\bar{\omega}$ is essentially independent of $\bar{q}$. This is the characteristic behavior of the sound attenuation coefficient of a Landau Fermi liquid in the collisionless thermal regime (see Table II). To determine the temperature dependence of the attenuation in this regime, in Fig. 8 we plot the logarithm of the ratio $\mathrm{Im}\bar{\omega}(T)/\mathrm{Im}\bar{\omega}(0)$ versus the logarithm of $\tilde{d}^{-1/3} \sim T/\mu$ at fixed $\bar{q} = 0.01$. In the collisionless quantum regime, the attenuation is essentially temperature independent, whereas in the collisionless thermal regime it scales as $\sim T^2$. The transition occurs at $\bar{q} \sim \tilde{d}^{-1/3}$. This is fully compatible with LFL behavior (see

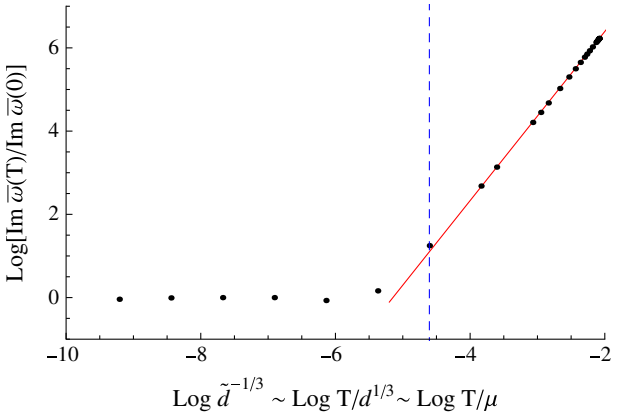

FIG. 8 (color online). The imaginary part of the holographic zero sound dispersion relation at low temperatures showing the transition between the collisionless quantum (left) and collisionless thermal (right) regimes. The points are the numerical data, the dashed line denotes $\bar{q} = \tilde{d}^{-1/3} \sim T/\mu$, and the solid line is the best-fit straight line for the $T/\mu \gtrsim \bar{q} = 0.01$ points showing the $\sim T^2$ scaling of the attenuation in the collisionless thermal regime. The region corresponding to the hydrodynamic regime at even higher temperature $T/\mu \gg \sqrt{\bar{q}} = 0.1$ is not shown in the figure.

Table II and Fig. 3). Figure 8 should be compared to the transition between regions II and III in Fig. 3.

At nonzero hypermultiplet mass the results are qualitatively the same and the plots for $\bar{m} = 0.76$, 1.68 are similar to Fig. 8. We do not show these plots for conciseness.

Another comparison with Landau Fermi-liquid theory can be made by plotting the attenuation as a function of (real) frequency. As shown in Fig. 2 and Table II, in the frequency dependence of the acoustic attenuation, the transition from the collisionless thermal regime to the collisionless quantum regime is characterized by a change of scaling from $\arg(q) \propto 1/\omega$ to $\arg(q) \propto \omega$ at $\bar{\omega} \sim T/\mu$. We can study this region in the D3/D7 system by fixing the temperature (at e.g. $\tilde{d} = 10^4$) and tracing the Green's function's pole in the complex momentum plane while varying the real frequency $\bar{\omega}$. The results are shown in Fig. 9 for the massless case. In the collisionless quantum regime, the points follow a straight line with gradient 1. In the collisionless thermal regime, for a region where there is a power law dependence $\arg(\bar{q}) \propto \bar{\omega}^{\alpha}$, the best-fit value of α turns out to be $\alpha \approx -0.95$, which is sufficiently close to the LFL value of -1. Figure 9 can be compared to regions II and III in Fig. 2. As we approach the hydrodynamic regime, the power law dependence is lost as expected. We are not able to explore the acoustic mode in region I due to limitations of the probe brane approximation, as explained in the introduction. The best-fit gradients are the same for nonzero masses $\bar{m} = 0.76$, 1.68 and so they are not shown here for brevity.

C. The collisionless-hydrodynamic crossover

As the temperature is increased further, the zero sound mode becomes less stable, and the system enters the hydrodynamic regime characterized by

$$0 \leq \bar{\omega}, \bar{q} \ll \tilde{d}^{-2/3}. \tag{34}$$

The zero sound peak in the spectral function broadens and moves to the origin (see Fig. 10). The real and imaginary parts of the collective mode's dispersion relation as functions of temperature are shown in Fig. 11 for massless and massive hypermultiplets. The real part decreases with increasing temperature until it becomes exactly zero at $T = T_{\text{cross}}$, and the mode ceases to propagate. The magnitude of the imaginary part increases until $T = T_{\text{cross}}$, then decreases again. For $T > T_{\text{cross}}$, the mode is purely diffusive, approaching at high temperatures the known analytic result (28) for the hydrodynamic charge density diffusion mode. The transition occurs at $\bar{q} \sim \tilde{d}^{-2/3}$, as we will shortly show.

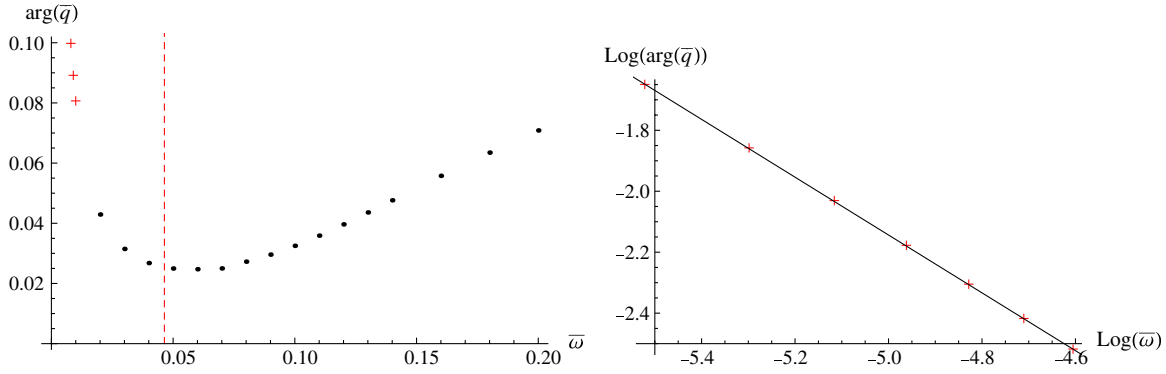

FIG. 9 (color online). The frequency dependence of the D3/D7 acoustic mode when $\bar{m} = 0$, $\tilde{d} = 10^4$ in the collisionless regimes. The dots and crosses are our numerical results, the dashed line is $\bar{\omega} = \pi T/d^{1/3} \sim T/\mu$, and the solid line shows the best-fit straight line with gradient $\alpha \approx -0.95$. The points on the left of the left-hand plot correspond to the rightmost points on the right-hand plot.

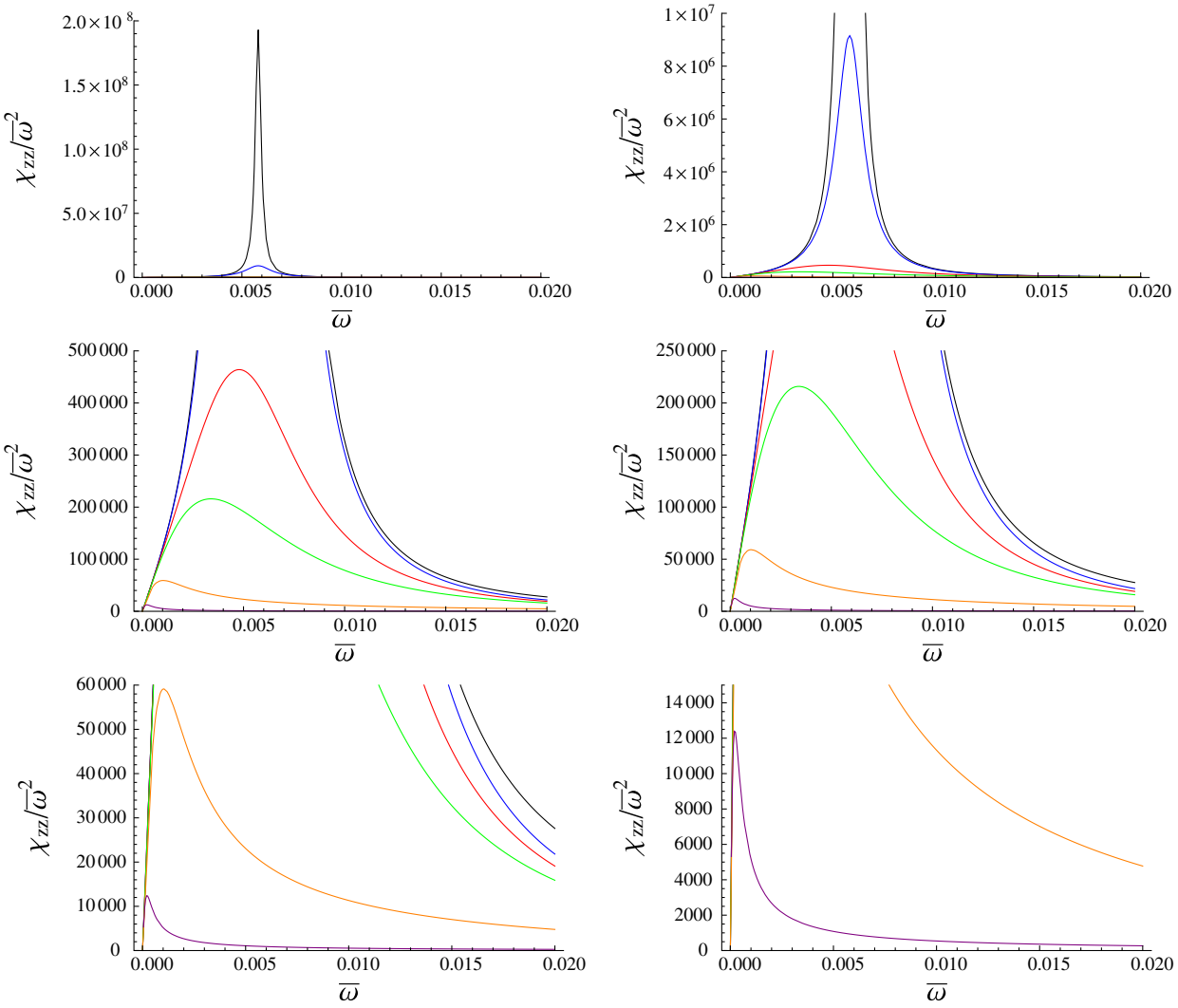

FIG. 10 (color online). The longitudinal spectral functions for $\bar{m} = 0$, $\bar{q} = 0.01$. Moving from the top left corner to the bottom right corner: each subsequent figure zooms into the area of detail in the previous one (note the different scales on the vertical axes). In each figure, moving from the tallest peak to the smallest peak corresponds to raising the temperature: $\tilde{d} = 10^5$ (black), 10^4 (blue), 10^3 (red), 500 (green), 100 (orange), and 10 (purple).

The dynamics of this collisionless-hydrodynamic transition are best exhibited by the motion of the relevant poles in the complex frequency plane (see Fig. 12). As the temperature is raised, the two zero sound poles (corresponding to $\mathrm{Re}\bar{\omega} = \pm v_s \bar{q}$) move deeper into the complex plane, approximately along the circle $|\bar{\omega}| = \bar{q}/\sqrt{3}$, until they collide on the imaginary axis and form two purely imaginary poles. (For the parameters used in Fig. 12, this happens at $\tilde{d} = \tilde{d}_{\mathrm{cross}} \approx 519$, i.e., in the region $\bar{q} \sim \tilde{d}^{-2/3}$.) One of these new poles recedes quickly into the complex plane as the temperature is raised further, while the other approaches the real axis and becomes the hydrodynamic diffusion mode (28) at high temperatures. This explains the temperature dependence of the collective mode dispersion relation in Fig. 11 and the behavior of the density-density spectral function in Fig. 10. At nonzero hypermultiplet mass, the transition is qualitatively similar, although the transition temperature decreases slightly with increasing mass ($\tilde{d}_{\mathrm{cross}} \approx 520$, 530 for $\bar{m} = 0.76$, 1.68, respectively).

The phenomenon in which two poles on the imaginary axis collide and generate two propagating modes persists at lower densities as well [in fact, it was first observed in Fig. 3(c) of [31] for $\tilde{d} = 2$ which is the highest value of $\tilde{d}$ studied in that paper], although in the low density regime the pole collision occurs deep in the complex plane and the propagating mode is short lived. The pole merger has also been recently observed and correctly identified as the hydrodynamic-collisionless transition involving the zero sound in a (2 + 1)-dimensional theory in [23].

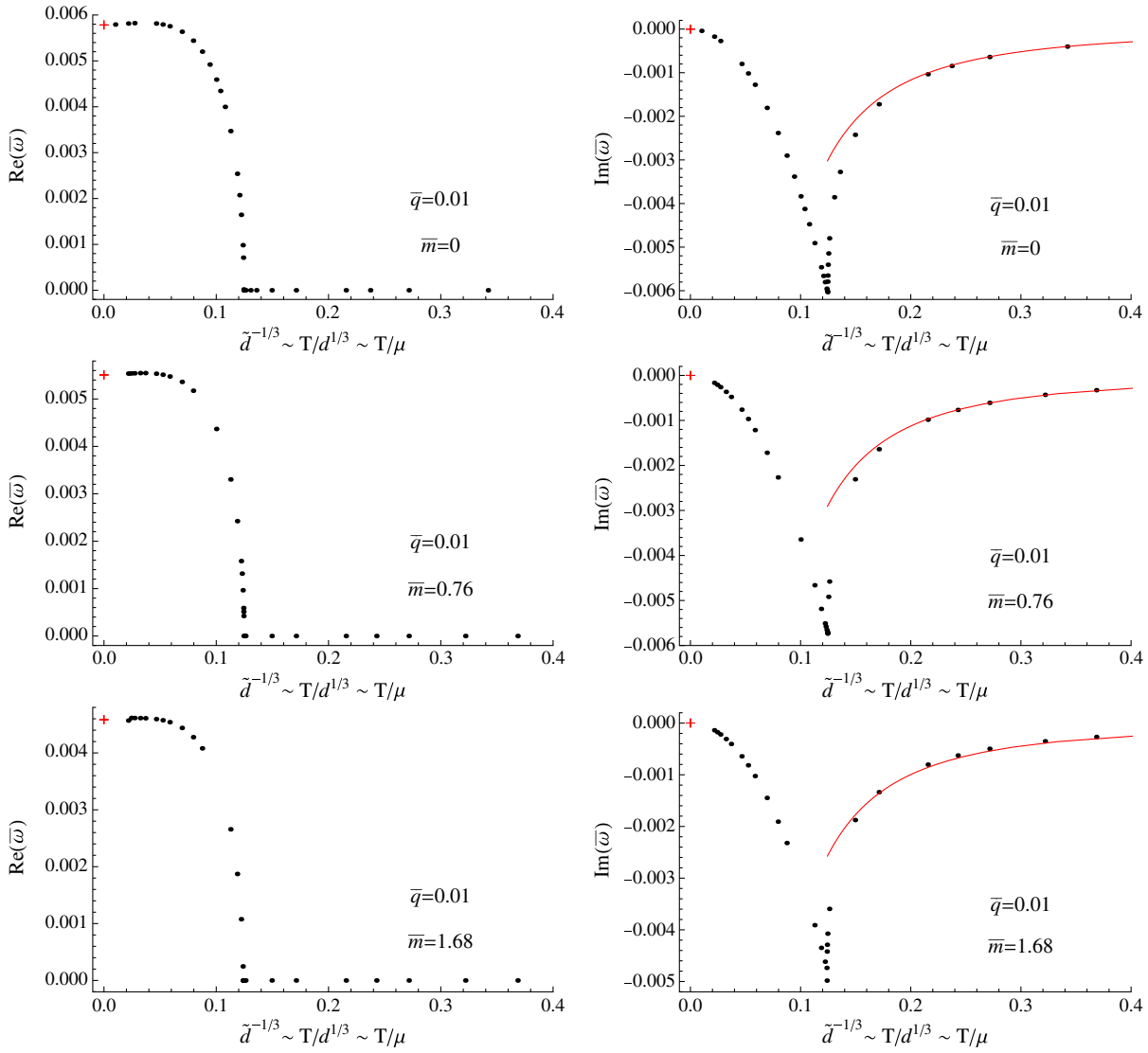

FIG. 11 (color online). The temperature dependence of the real and imaginary parts of the dominant collective mode's dispersion relation at $\bar{q} = 0.01$ and $\bar{m} = 0$; 0.76; 1.68. Dots show the numerical results at low T, the crosses show the $T = 0$ zero sound results (27) and (30), and the solid lines show the analytic diffusion result (28).

In Landau Fermi-liquid theory, the collisionless-hydrodynamic transition occurs when $\omega\tau \sim 1$ and $ql_{\mathrm{mfp}} \sim 1$, where τ and l_{mfp} are the mean free time and mean free path, respectively, of the quasiparticles in the vicinity of the Fermi surface supporting the collective mode. Defining the collisionless-hydrodynamic transition in the D3/D7 holographic model as the event in which the two poles in Fig. 12 merge, we can cast the corresponding parameters in the familiar language of the Landau theory by introducing an effective $\tau = 1/|\omega_{\mathrm{cross}}|$ and $l_{\mathrm{mfp}} = 1/q_{\mathrm{cross}}$, and computing their temperature dependence. Assuming a simple power dependence of the form

$$l_{\mathrm{mfp}} \sim \tau \propto d^{-1/3}\left(\frac{T}{d^{1/3}}\right)^{\alpha}, \tag{35}$$

we expect a plot of $\log(\bar{q}_{\mathrm{cross}})$ or $\log(|\bar{\omega}_{\mathrm{cross}}|)$ versus $\log(\tilde{d}^{1/3}_{\mathrm{cross}})$ to yield a straight line of gradient α. These plots are shown in Fig. 13 for the massless case. The numerical results are clearly consistent with a simple power law dependence. The slope of the best-fit straight line is -2.0 in each case, which leads to the result

$$l_{\mathrm{mfp}} \sim \tau \sim d^{1/3}T^{-2} \sim \mu T^{-2}, \tag{36}$$

as in a Landau Fermi liquid [16]; recall Table I. For nonzero masses $\bar{m} = 0.76$, 1.68, the best-fit slopes are unchanged and so we do not show the results for brevity.

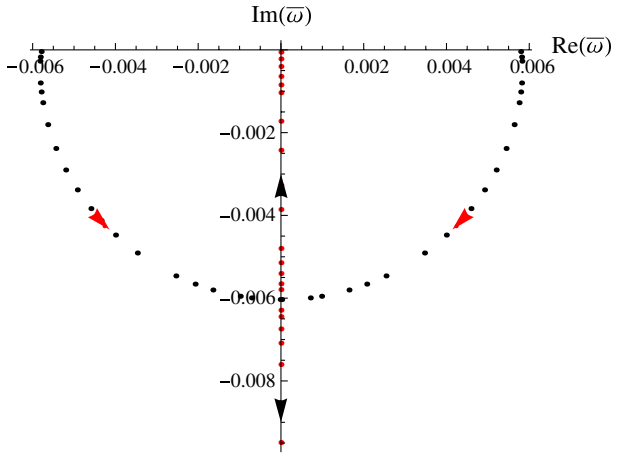

FIG. 12 (color online). The positions of the dominant poles of the density-density correlator in the complex frequency plane at $\bar{m} = 0$, $\bar{q} = 0.01$ as the temperature is changed. The low temperature limit corresponds to the points farthest from the imaginary axis. As the temperature is increased, the points move inward toward the imaginary axis where they collide to form two poles that move up and down the imaginary axis, respectively. See Supplemental Material at [62] for an animated version of this figure and the corresponding animations for $\bar{m} = 0.76$, 1.68.

IV. SUMMARY AND DISCUSSION

In this paper, we have investigated the properties of the holographic zero sound mode and the fundamental matter diffusion mode in the D3/D7 system at finite temperature and high density. Similar to the case of an ordinary Landau Fermi liquid, three regimes corresponding to different powers of the parameter $T/\mu \ll 1$ can be identified, with the modes having a distinctively different temperature and momentum dependence in each regime. In the collisionless quantum regime, the zero sound attenuation is essentially temperature independent and proportional to the square of the momentum, whereas in the collisionless thermal regime, the attenuation is momentum independent and scales as the square of the temperature (see Table II, Figs. 2 and 3 and the corresponding D3/D7 results in Figs. 8 and 9). The crossover transition between the two regimes is clearly visible in Figs. 8 and 9. In the hydrodynamic regime of a Landau Fermi liquid, the acoustic attenuation is proportional to the square of the momentum and scales as $\sim 1/T^2$. Restricted by the probe brane approximation, we are unable to study the acoustic collisionless-hydrodynamic crossover transition in the D3/D7 theory directly.[7] However, we do observe this transition in the density-density correlator as the motion of the lowest-lying poles in the complex frequency plane leads from the zero sound-dominated regime to the diffusion-dominated one as the parameter T/μ is increased (Fig. 12). The transition occurs at ω, $q \sim T^2/\mu$, as if it were supported by Landau Fermi-liquid quasiparticles with a lifetime $\sim 1/T^2$. These results do not qualitatively change as the mass of the fundamental matter in the field theory is varied, at least in the range $0 \leq \bar{m} \leq 1.68$ which we have studied numerically.

The main conclusion of our study is that the holographic zero sound of the D3/D7 system at finite temperature behaves exactly as the usual Landau zero sound. This is rather difficult to reconcile, at least within the standard Landau Fermi-liquid paradigm, with two other properties of the system: the atypical temperature dependence of the specific heat ($c_V \propto T^6/d$ instead of $c_V \propto Td^{2/3}$) and the apparent absence of a singularity when $|\vec{q}| = 2q_F$ at zero frequency in the density-density correlator at zero temperature. One may add to these apparent discrepancies a finite zero-temperature limit of the entropy density [11]. Resolution of the above mentioned puzzles may involve modifications of the gravitational background considered, possibly in the spirit of [56]. On the other hand, the absence of the singularity in the zero frequency density-density correlator at $2k_F$ may have a simpler explanation[8]: assuming the validity of the Luttinger theorem, $n_q \sim k_F^3$, and therefore $q \sim 2k_F \sim n_q^{1/3} \sim d^{1/3}\lambda^{1/6}$, since $d \sim n_q/\sqrt{\lambda}$. This means that the corresponding $\bar{q}$ is large, $\bar{q} \sim \lambda^{1/6}$, and is not visible in the correlators in the probe brane limit. It is also possible that the $\sim T^6$ behavior of the specific heat is a genuine property of the considered microscopic model in the approximation described by the probe brane limit, there is no Fermi surface, and we are dealing with a new type of quantum liquid. This point of view, initially advocated in [11], is not in contradiction with the findings presented in our paper.

There are other examples of theories with a dual holographic description which support a sound mode at $T = 0$. It would be interesting to determine whether the results presented here hold (qualitatively) in those cases also. The first class of such theories are probe brane theories [21–25]. Of particular interest are the D4/D8/$\overline{\text{D8}}$ theory, whose sound mode has a different dispersion relation from Landau Fermi-liquid theory at $T = 0$, and the D3/D3 theory which is $(1 + 1)$ dimensional and hence to which Landau Fermi-liquid theory does not apply. A qualitatively different holographic theory is the AdS_4 Einstein-Maxwell theory at finite density [26,57–61]. In this theory, nontrivial density-dependent physics is possible via the strong coupling of the charge density to the energy density of the field theory. This is in contrast to probe theories, where the DBI coupling between the charge density gives rise to interesting density-dependent physics, despite the fact that the coupling of this sector to the overall energy density is

[7] See [55] for some recent work on going beyond the probe approximation.

[8] We are indebted to Andrei Parnachev and Pavel Kovtun for valuable discussions on this issue.

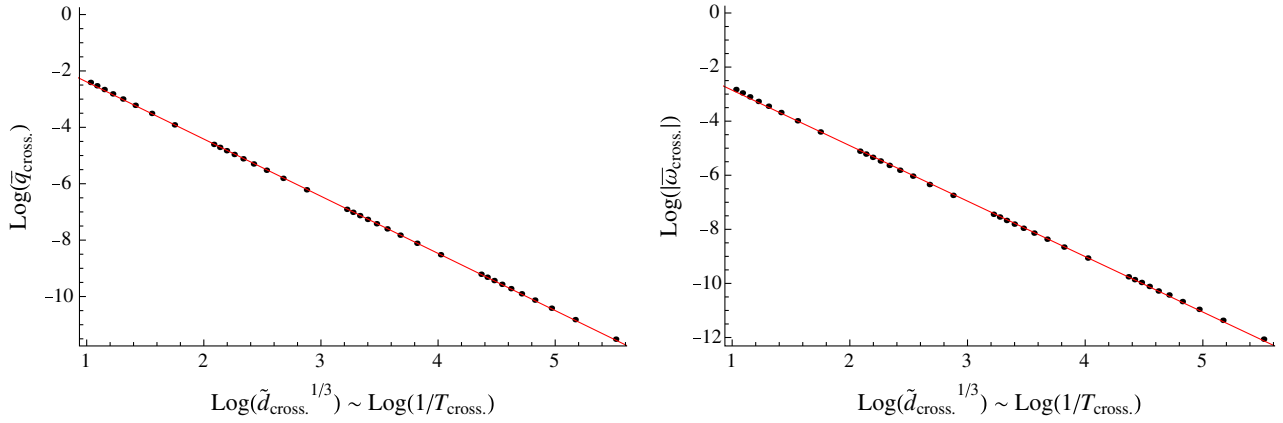

FIG. 13 (color online). The temperature dependence of the collisionless-hydrodynamic crossover value of frequency and momentum for $\bar{m} = 0$. The points are our numerical results and the solid lines are the best-fit straight lines which both have gradient -2.0.

suppressed via the probe limit. These are very different mechanisms and hence it would be very interesting to see if the low temperature sound mode in the Einstein-Maxwell theory behaves similarly to the corresponding sound mode in the D3/D7 theory.

Finally, it would be very interesting to generalize the recent approach to zero sound proposed in [47] to nonzero temperatures.

ACKNOWLEDGMENTS

We would like to thank Andy O'Bannon for useful discussions and for bringing Fig. 3 of Ref. [31] to our attention. A. O. S. thanks Johanna Erdmenger, Kristan Jensen, Chris Herzog, Pavel Kovtun, Manuela Kulaxizi, Andrei Parnachev, Giuseppe Policastro, Mukund Rangamani, Eva Silverstein, Dam Thanh Son, and Jan Zaanen for helpful discussions and comments on the manuscript, and KITP for hospitality during the very last phase of the project. The work of R. A. D. was supported by the UK Science and Technology Facilities Council (STFC). The work of A. O. S. was supported, in part, by STFC.

APPENDIX A: FLUCTUATIONS AT NONZERO HYPERMULTIPLET MASS

When the hypermultiplet has a nonzero mass, the bulk fluctuations of the embedding scalar and the longitudinal gauge field components are coupled and their solutions are no longer independent. In the field theory, this corresponds to mixing of the dual operators. An appropriate systematic formalism which we follow was introduced in [31]. It will be convenient to work with the gauge-invariant variables

$$\begin{aligned}\varphi(u,\bar{\omega}) &= r_H\tilde{\phi}(u,\bar{\omega}),\\ \bar{E}(u,\bar{\omega}) &= -i[\bar{\omega}\tilde{a}_z(u,\bar{\omega}) + \bar{q}\tilde{a}_t(u,\bar{\omega})].\end{aligned} \tag{A1}$$

Note that the definition of $\bar{E}$ differs from the massless case (21) by a factor of $-i$. The coupled system of equations of motion for the variables $\bar{E}$ and φ is

$$\begin{aligned}&\frac{d}{du}\left(\frac{f(u)\cos^3\theta}{\sqrt{G(u)}D(u,\bar{\omega})}[H(u)\bar{E}'(u,\bar{\omega}) + 4i\bar{q}f(u)u^2\theta'(u)A(u)\varphi'(u,\bar{\omega}) + 3i\bar{q}\tan\theta A(u)G(u)\varphi(u,\bar{\omega})]\right)\\ &\quad + \frac{\tilde{d}^{2/3}\cos^3\theta H(u)}{4uf(u)\sqrt{G(u)}}\bar{E}(u,\bar{\omega}) + \frac{\tilde{d}^{2/3}\cos^3\theta uA(u)\theta'(u)}{\sqrt{G(u)}}i\bar{q}\varphi(u,\bar{\omega}) = 0,\end{aligned} \tag{A2}$$

and

$$\begin{aligned}&\frac{d}{du}\left(\frac{f(u)\cos^3\theta}{u\sqrt{G(u)}D(u,\bar{\omega})}[(\bar{\omega}^2 - \bar{q}^2f(u)B(u))\varphi'(u,\bar{\omega}) - 4i\bar{q}f(u)u^3\theta'(u)A(u)\bar{E}'(u,\bar{\omega}) - 3\tan\theta\theta'(u)G(u)(\bar{\omega}^2 - \bar{q}^2f(u))\varphi(u,\bar{\omega})]\right)\\ &\quad + \frac{3\cos^2\theta\sin\theta f(u)A(u)\sqrt{G(u)}}{D(u,\bar{\omega})}i\bar{q}\bar{E}'(u,\bar{\omega}) - \frac{\cos^3\theta uA(u)\theta'(u)\tilde{d}^{(2/3)}}{\sqrt{G(u)}}i\bar{q}\,\bar{E}(u,\bar{\omega})\\ &\quad + \frac{3\cos^2\theta\sin\theta f(u)\theta'(u)\sqrt{G(u)}(\bar{\omega}^2 - \bar{q}^2f(u))}{uD(u,\bar{\omega})}\varphi'(u,\bar{\omega}) + \frac{\cos^3\theta\tilde{d}^{(2/3)}(\bar{\omega}^2 - \bar{q}^2f(u)B(u))}{4u^2f(u)\sqrt{G(u)}}\varphi(u,\bar{\omega})\\ &\quad - \frac{9\cos\theta\sin^2\theta A(u)^2\sqrt{G(u)}\bar{\omega}^2}{D(u,\bar{\omega})}\varphi(u,\bar{\omega}) + \frac{3(3\cos^3\theta - 2\cos\theta)\sqrt{G(u)}}{4u^3}\varphi(u,\bar{\omega}) = 0,\end{aligned} \tag{A3}$$

where the coefficients are given by

$$A(u) = \frac{A_t'(u)}{r_H}, \qquad B(u) = 1 - 4u^3A(u)^2, \qquad G(u) = 1 + 4u^2f(u)\theta'(u)^2 - 4u^3A(u)^2,$$
$$H(u) = 1 + 4f(u)u^2\theta'(u)^2, \qquad D(u,\bar{\omega}) = \bar{\omega}^2H(u) - \bar{q}^2f(u)G(u),$$

and primes denote derivatives with respect to u.

The relevant part of the off-shell action quadratic in longitudinal fluctuations is

$$S^{(2)}_{\text{long}} = -Nr_H^2\int_0^1 du\frac{d\omega dq}{(2\pi)^2}\Big\{-\frac{\cos^3\theta f(u)H(u)}{\sqrt{G(u)}D(u,\bar{\omega})}\bar{E}'(u,-\bar{\omega})\bar{E}'(u,\bar{\omega}) - \frac{8\cos^3\theta f(u)^2u^2\theta'(u)A(u)}{\sqrt{G(u)}D(u,\bar{\omega})}i\bar{q}\bar{E}'(u,-\bar{\omega})\varphi'(u,\bar{\omega})$$
$$- \frac{\cos^3\theta f(u)(\bar{\omega}^2 - \bar{q}^2f(u)B(u))}{u\sqrt{G(u)}D(u,\bar{\omega})}\varphi'(u,-\bar{\omega})\varphi'(u,\bar{\omega}) + \frac{6\cos^2\theta\sin\theta f(u)A(u)\sqrt{G(u)}}{D(u,\bar{\omega})}i\bar{q}\varphi(u,-\bar{\omega})\bar{E}'(u,\bar{\omega})$$
$$+ \frac{6\cos^2\theta\sin\theta f(u)\theta'(u)\sqrt{G(u)}(\bar{\omega}^2 - \bar{q}^2f(u))}{uD(u,\bar{\omega})}\varphi(u,-\bar{\omega})\varphi'(u,\bar{\omega}) + \text{nonderivative terms}\Big\}, \tag{A4}$$

where $N = N_fT_{\text{D7}}V_{S^3}$. The equations of motion and the action are written in the form that allow one to apply the recipes of [31] directly. To obtain the retarded Green's functions, we solve the coupled system of equations (A2) and (A3) with incoming wave boundary conditions at the horizon and combine with the appropriate factors from the action (A4) as described in [31].

APPENDIX B: HOLOGRAPHIC ZERO SOUND ATTENUATION AT FINITE HYPERMULTIPLET MASS AND ZERO TEMPERATURE

In this Appendix we derive the formula for the zero sound attenuation at finite hypermultiplet mass following the approach of Ref. [20]. Note that our notation is different from that used there. At zero temperature and nonzero mass, it will be convenient to use the coordinate system in which the background metric takes the form

$$ds_{10}^2 = \frac{r^2}{R^2}(-dt^2 + d\vec{x}^2) + \frac{R^2}{r^2}(d\rho^2 + \rho^2ds_{S^3}^2 + d\mathcal{R}^2 + \mathcal{R}^2d\phi^2),$$

where $r^2 = \rho^2 + \mathcal{R}^2$. The background DBI action is given by

$$S_{\text{fund}} = -N\int_0^\infty d\rho d^4x\rho^3\sqrt{1 + \mathcal{R}'(\rho)^2 - A_t'(\rho)^2},$$

where $\mathcal{R}$ is the embedding coordinate of the D7-branes. The background gauge field and embedding coordinate are determined by two conserved charges c and d via

$$A_t(\rho) = \frac{R^2}{6}d(d^2 - c^2)^{-(1/3)}\mathcal{B}\Big[\frac{\rho^6}{\rho^6 + d^2R^{12} - c^2R^{12}};\frac{1}{6},\frac{1}{3}\Big],$$
$$\mathcal{R}(\rho) = \frac{R^2}{6}c(d^2 - c^2)^{-(1/3)}\mathcal{B}\Big[\frac{\rho^6}{\rho^6 + d^2R^{12} - c^2R^{12}};\frac{1}{6},\frac{1}{3}\Big],$$

where d is the density of fundamental matter and $\mathcal{B}$ is the incomplete beta function. The mass and chemical potential are given by the asymptotic values

$$A_t(\rho\to\infty) = r_H\tilde{\mu}, \qquad \mathcal{R}(\rho\to\infty) = \frac{r_H}{\sqrt{2}}\tilde{m},$$

and are related to the constants d and c via

$$c = r_H^3\gamma\frac{\tilde{m}}{\sqrt{2}}(\tilde{\mu}^2 - \tilde{m}^2/2), \qquad d = r_H^3\gamma\tilde{\mu}(\tilde{\mu}^2 - \tilde{m}^2/2),$$

where

$$\gamma = \Big(\frac{R^2}{6}\mathcal{B}\Big[\frac{1}{6},\frac{1}{3}\Big]\Big)^{-3}.$$

The equations of motion for the fluctuations of the embedding scalar $\delta\mathcal{R}$ and the fluctuations of the gauge-invariant combination $\delta\mathcal{A} \equiv R^2\omega a_z + R^2qa_t$ are coupled.[9] In the near-horizon limit $\rho\to 0$, the solutions take the form

$$\delta\mathcal{A} = A\rho e^{\pm i\Omega/\rho}, \qquad \delta\mathcal{R} = B\rho e^{\pm i\Omega/\rho}, \tag{B1}$$

where $\Omega = R^2\omega\sqrt{1 - c^2/d^2}$ and the upper sign in the exponent corresponds to the ingoing boundary condition. In the small frequency limit ($\Omega/\rho \ll 1$), the solutions (B1) can be expanded as

$$\delta\mathcal{A} = \pm i\Omega A + A\rho + \cdots,$$
$$\delta\mathcal{R} = \pm i\Omega B + B\rho + \cdots. \tag{B2}$$

Alternatively, taking first the small frequency limit of the equations of motion, we obtain the following solutions near the boundary:

[9] They are given by Eqs. (A.11) of [20], with the replacements $E\to\delta\mathcal{A}$, $\xi\to\delta\mathcal{R}$, $r\to\rho$, $d\to dR^6$, $c\to cR^6$, $L\to R$, and $R\to\mathcal{R}$.

$$\delta\mathcal{A} = C_0 + O(1/\rho^2), \qquad \delta\mathcal{R} = \tilde{C}_0 + O(1/\rho^2),$$

whereas near the horizon the corresponding solutions are

$$\begin{aligned}\delta\mathcal{A} &= C_0 + b_1 C_1 + b_2 C_2 + a_1 C_1 \rho + a_2 C_2 \rho,\\ \delta\mathcal{R} &= \tilde{C}_0 + \tilde{b}_1 C_1 + \tilde{b}_2 C_2 + \tilde{a}_1 C_1 \rho + \tilde{a}_2 C_2 \rho,\end{aligned} \tag{B3}$$

where the coefficients are given by

$$a_1 = -\frac{c^2 q^2 + (d^2 - c^2)\omega^2}{R^2 (d^2 - c^2)^{3/2}}, \qquad a_2 = \frac{c d q^2}{R^2 (d^2 - c^2)^{3/2}},$$

$$b_1 = \frac{\Gamma(\frac{7}{6})\Gamma(\frac{4}{3})[(3c^2 - d^2)q^2 + 3(d^2 - c^2)\omega^2]}{\Gamma(\frac{1}{2})(d^2 - c^2)^{4/3}},$$

$$b_2 = -\frac{2 c d q^2 \Gamma(\frac{7}{6})\Gamma(\frac{4}{3})}{\Gamma(\frac{1}{2})(d^2 - c^2)^{4/3}}, \qquad \tilde{a}_1 = -\frac{c d}{R^6 (d^2 - c^2)^{3/2}},$$

$$\tilde{a}_2 = \frac{d^2}{R^6 (d^2 - c^2)^{3/2}}, \qquad \tilde{b}_1 = \frac{2 c d \Gamma(\frac{7}{6})\Gamma(\frac{4}{3})}{R^4 \Gamma(\frac{1}{2})(d^2 - c^2)^{4/3}},$$

$$\tilde{b}_2 = -\frac{\Gamma(\frac{7}{6})\Gamma(\frac{4}{3})(3d^2 - c^2)}{R^4 \Gamma(\frac{1}{2})(d^2 - c^2)^{4/3}}.$$

The poles of the retarded Green's function correspond to the quasinormal modes of the system—these are the solutions which obey ingoing boundary conditions near the horizon and vanish near the boundary. Such solutions exist when it is possible to match the expansion (B2) (with the upper sign) onto the expansion (B3) with $C_0 = \tilde{C}_0 = 0$. Performing this matching order by order in ρ, we find that the coefficients C_1 and C_2 obey the equation

$$\begin{pmatrix} i\Omega a_1 - b_1 & i\Omega a_2 - b_2 \\ i\Omega \tilde{a}_1 - \tilde{b}_1 & i\Omega \tilde{a}_2 - \tilde{b}_2 \end{pmatrix} \begin{pmatrix} C_1 \\ C_2 \end{pmatrix} = \begin{pmatrix} 0 \\ 0 \end{pmatrix}. \tag{B4}$$

A nontrivial solution exists provided that

$$\begin{vmatrix} i\Omega a_1 - b_1 & i\Omega a_2 - b_2 \\ i\Omega \tilde{a}_1 - \tilde{b}_1 & i\Omega \tilde{a}_2 - \tilde{b}_2 \end{vmatrix} = 0. \tag{B5}$$

By substituting an expansion of the form $\omega = c_0 + c_1 q + c_2 q^2 + \cdots$, we find that the above determinant vanishes when ω is given by the dispersion relation (30). Note that this method finds only the lowest energy quasinormal modes, as it involves taking the small ω limit.

[1] J. M. Maldacena, Adv. Theor. Math. Phys. **2**, 231 (1998).
[2] S. S. Gubser, I. R. Klebanov, and A. M. Polyakov, Phys. Lett. B **428**, 105 (1998).
[3] E. Witten, Adv. Theor. Math. Phys. **2**, 253 (1998).
[4] O. Aharony, S. S. Gubser, J. M. Maldacena, H. Ooguri, and Y. Oz, Phys. Rep. **323**, 183 (2000).
[5] D. T. Son and A. O. Starinets, Annu. Rev. Nucl. Part. Sci. **57**, 95 (2007).
[6] J. Casalderrey-Solana, H. Liu, D. Mateos, K. Rajagopal, and U. Achim Wiedemann, arXiv:1101.0618.
[7] S. A. Hartnoll, Classical Quantum Gravity **26**, 224002 (2009).
[8] C. P. Herzog, J. Phys. A **42**, 343001 (2009).
[9] J. McGreevy, Adv. High Energy Phys. **2010**, 723105 (2010) .
[10] A. Karch and E. Katz, J. High Energy Phys. 06 (2002) 043.
[11] A. Karch, D. T. Son, and A. O. Starinets, Phys. Rev. Lett. **102**, 051602 (2009).
[12] L. D. Landau, Zh. Eksp. Teor. Fiz. **32**, 59 (1957) [Sov. Phys. JETP **5**, 101 (1959)].
[13] E. M. Lifshitz and L. P. Pitaevskii, *Course of Theoretical Physics: Statistical Physics Part 2* (Pergamon Press, Oxford, 1980), Vol. 9.
[14] E. M. Lifshitz and L. P. Pitaevskii, *Course of Theoretical Physics: Physical Kinetics* (Pergamon Press, Oxford, 1981), Vol. 10.
[15] A. A. Abrikosov, L. P. Gorkov, and I. E. Dzyaloshinski, *Methods of Quantum Field Theory in Statistical Physics* (Dover, New York, 1968).
[16] D. Pines and P. Nozières, *The Theory of Quantum Liquids* (W. A. Benjamin, New York, 1966).
[17] A. A. Abrikosov and I. M. Khalatnikov, Rep. Prog. Phys. **22**, 329 (1959).
[18] W. R. Abel, A. C. Anderson, and J. C. Wheatley, Phys. Rev. Lett. **17**, 74 (1966).
[19] E. R. Dobbs, *Helium Three* (Oxford University Press, Oxford, 2000).
[20] M. Kulaxizi and A. Parnachev, Phys. Rev. D **78**, 086004 (2008).
[21] M. Kulaxizi and A. Parnachev, Nucl. Phys. **B815**, 125 (2009).
[22] L.-Y. Hung and A. Sinha, J. High Energy Phys. 01 (2010) 114.
[23] O. Bergman, N. Jokela, G. Lifschytz, and M. Lippert, J. High Energy Phys. 10 (2011) 034.
[24] C. Hoyos-Badajoz, A. O'Bannon, and J. M. S. Wu, J. High Energy Phys. 09 (2010) 086.
[25] B.-H. Lee, D.-W. Pang, and C. Park, J. High Energy Phys. 11 (2010) 120.
[26] M. Edalati, J. I. Jottar, and R. G. Leigh, J. High Energy Phys. 10 (2010) 058.
[27] K.-Y. Kim and I. Zahed, J. High Energy Phys. 12 (2008) 075.
[28] C. P. Herzog, P. Kovtun, S. Sachdev, and D. T. Son, Phys. Rev. D **75**, 085020 (2007).
[29] I. Amado, C. Hoyos-Badajoz, K. Landsteiner, and S. Montero, Phys. Rev. D **77**, 065004 (2008).
[30] I. Amado, C. Hoyos-Badajoz, K. Landsteiner, and S. Montero, J. High Energy Phys. 07 (2008) 133.
[31] M. Kaminski, K. Landsteiner, J. Mas, J. P. Shock, and J. Tarrio, J. High Energy Phys. 02 (2010) 021.
[32] M. Kaminski *et al.*, J. High Energy Phys. 03 (2010) 117.

[33] C. P. Herzog, Phys. Rev. D **81**, 126009 (2010).
[34] S. Kobayashi, D. Mateos, S. Matsuura, R. C. Myers, and R. M. Thomson, J. High Energy Phys. 02 (2007) 016.
[35] J. Mas, J. P. Shock, and J. Tarrio, J. High Energy Phys. 01 (2009) 025.
[36] M. Kruczenski, D. Mateos, R. C. Myers, and D. J. Winters, J. High Energy Phys. 07 (2003) 049.
[37] A. Karch and A. O'Bannon, J. High Energy Phys. 11 (2007) 074.
[38] M. C. Wapler, J. High Energy Phys. 05 (2010) 019.
[39] D. Mateos, R. C. Myers, and R. M. Thomson, J. High Energy Phys. 05 (2007) 067.
[40] S. Nakamura, Y. Seo, S.-J. Sin, and K. P. Yogendran, Prog. Theor. Phys. **120**, 51 (2008).
[41] K. Ghoroku, M. Ishihara, and A. Nakamura, Phys. Rev. D **76**, 124006 (2007).
[42] T. Faulkner and H. Liu, arXiv:0812.4278.
[43] D. Mateos, S. Matsuura, R. C. Myers, and R. M. Thomson, J. High Energy Phys. 11 (2007) 085.
[44] P. K. Kovtun and A. O. Starinets, Phys. Rev. D **72**, 086009 (2005).
[45] D. T. Son and A. O. Starinets, J. High Energy Phys. 09 (2002) 042.
[46] R. C. Myers, A. O. Starinets, and R. M. Thomson, J. High Energy Phys. 11 (2007) 091.
[47] D. Nickel and D. T. Son, New J. Phys. **13**, 075010 (2011).
[48] D. Mateos, R. C. Myers, and R. M. Thomson, Phys. Rev. Lett. **97**, 091601 (2006).
[49] C. Hoyos-Badajoz, K. Landsteiner, and S. Montero, J. High Energy Phys. 04 (2007) 031.
[50] A. Paredes, K. Peeters, and M. Zamaklar, J. High Energy Phys. 05 (2008) 027.
[51] J. Erdmenger, M. Kaminski, and F. Rust, Phys. Rev. D **77**, 046005 (2008).
[52] R. C. Myers and A. Sinha, J. High Energy Phys. 06 (2008) 052.
[53] J. Mas, J. P. Shock, J. Tarrio, and D. Zoakos, J. High Energy Phys. 09 (2008) 009.
[54] M. Ammon *et al.*, J. High Energy Phys. 09 (2011) 030.
[55] F. Bigazzi, A. L. Cotrone, J. Mas, D. Mayerson, and J. Tarrio, J. High Energy Phys. 04 (2011) 060.
[56] S. A. Hartnoll, J. Polchinski, E. Silverstein, and D. Tong, J. High Energy Phys. 04 (2010) 120.
[57] H. Liu, J. McGreevy, and D. Vegh, Phys. Rev. D **83**, 065029 (2011).
[58] T. Faulkner, H. Liu, J. McGreevy, and D. Vegh, Phys. Rev. D **83**, 125002 (2011).
[59] R. Belliard, S. S. Gubser, and A. Yarom, J. High Energy Phys. 10 (2011) 055.
[60] J. P. Gauntlett, J. Sonner, and D. Waldram, arXiv:1106.4694 [Phys. Rev. Lett. (to be published)].
[61] J. Gauntlett, J. Sonner, and D. Waldram, arXiv:1108.1205.
[62] See Supplemental Material at http://link.aps.org/supplemental/10.1103/PhysRevD.85.026004 for an animated version of this figure and the corresponding animations for $\bar{m} = 0.76, 1.68$.